Electronic Supplementary Information

Cascade Surface Immobilization Strategy to Access High-density and Closely-distanced Atomic Pt Sites for Enhancing Alkaline Hydrogen Evolution Reaction

Wenping Liu,[a] Jing Ji,[c] Xuecheng Yan,[b] Wenbo Liu,[a] Yu-Cheng Huang,[d] Kang Wang,*[a] Peng Jin,*[c] Xiangdong Yao[b] and Jianzhuang Jiang*[a]

[a] *Beijing Key Laboratory for Science and Application of Functional Molecular and Crystalline Materials, Department of Chemistry, University of Science and Technology Beijing, Beijing 100083, China*

[b] *Queensland Micro- and Nanotechnology Centre, Griffith University, Nathan Campus QLD 4111, Australia*

[c] *School of Materials Science and Engineering, Hebei University of Technology, Tianjin 300130, PR China*

[d] *Department of Physics, Tamkang University, 151 Yingzhuan Road, New Taipei City, 25137*

E-mail: kangwang@ustb.edu.cn (K.W.), china.peng.jin@gmail.com (P.J.), jianzhuang@ustb.edu.cn (J.J.)

Experimental Section

General Remarks. All chemicals were used as purchased without further purification unless otherwise specified. H_2TBPP, PtTBPP, RhTBPP, and PdTBPP were prepared according to published procedures.[S1]

Synthesis of PtSA@BP. Carbon black (BP 2000) powder (40 mg) was added into the THF solution of PtTBPP (25 ml, 0.3 mg mL^{-1}). The suspension was stirred for 12 h and the black product was collected by filtration, washed with ethanol and DI water, and dried under reduced pressure, affording the PtTBPP/BP hybrid (*ca.* 42 mg). The PtTBPP/BP hybrid was subsequently heated at 280°C for 1 h and then at 800 °C for another 2 h with a heating rate of 5°C min^{-1}, resulting in a product PtSA@BP (*ca.* 35 mg). ICP-AES analysis reveals a loading of 2.5 wt% for Pt in the as-prepared sample.

Following the above-described procedure with the THF solution of PtTBPP (25 ml, 0.05, 0.10, and 0.20 mg mL^{-1}) instead of PtTBPP (25 ml, 0.3 mg mL^{-1}), a series of PtSA@BP samples with the Pt loading of 0.4, 0.7, and 2.0 wt%, respectively, were prepared.

Synthesis of NBP. Also by means of the above-mentioned synthesis procedure for PtSA@BP with metal free H_2TBPP (25 ml, 0.3 mg mL^{-1}) instead of PtTBPP (25 ml, 0.3 mg mL^{-1}), the metal free nitrogen-doped sample NBP (*ca.* 32 mg) was synthesized.

Synthesis of RhSA@BP. Also by means of the above-mentioned synthesis procedure for

PtSA@BP with RhTBPP (25 ml, 0.3 mg mL^{-1}) instead of PtTBPP (25 ml, 0.3 mg mL^{-1}), RhSA@BP (*ca.* 33 mg) was synthesized.

Synthesis of PdSA@BP. Also by means of the above-mentioned synthesis procedure for PtSA@BP with PdTBPP (25 ml, 0.3 mg mL^{-1}) instead of PtTBPP (25 ml, 0.3 mg mL^{-1}), PdSA@BP (*ca.* 32 mg) was synthesized.

Scaled-up synthesis of PtSA@BP. By means of the synthesis procedure for PtSA@BP as mentioned above with increasing the dosage of all the reagents by 75 times, *ca*. 3000 mg PtSA@BP was obtained by one synthesis process.

Characterizations. HT7700 electron microscope at 100 KV was utilized for transmission electron microscopy (TEM) measurement. HAADF-STEM images and energy dispersive spectroscopy (EDS) mapping images were taken on a JEM-ARM200F electron microscope operated at 200 kV. AC STEM images were collected from TECNAI 12 and probe-corrected JEOL ARM200F with an acceleration voltage of 200 kV. Solid-state UV-Vis diffuse reflectance spectra were recorded on an SHIMADZU UV-2600 spectrophotometer. Solution-state UV-Vis absorption spectra were collected using a Perkin-Elmer Lambda 750 UV-vis spectrophotometer. Fluorescence analyses were carried out on a HITACHI F-4500 spectrometer. X-ray photoelectron spectra (XPS) were collected from PHI 5300 ESCA System (PerkineElmer, USA). N_2 adsorption-desorption isotherms were measured on a ASAP 2020 PLUS HD88 apparatus at 77 K and the surface areas were calculated by the Brunauere Emmette Teller (BET) method. TG-DSC

(NETZSCH STA 409 PC/PG) was applied to trace the weight loss in the carbonization stage. Raman spectra were recorded on a Rennishaw InVia spectrometer with a model 100 Ramascope optical fiber instrument. ICP-AES was performed on a Thermo IRIS Intrepid II XSP spectrometer. Before measurement, the samples were degassed in a vacuum at 120°C for 12 hours. XRD patterns were acquired at room temperature with a Shimadzu XRD-6000 diffractometer.

EXAFS measurement and data analysis. X-ray absorption spectra (XAS) were obtained at the National Synchrotron Radiation Research Center (NSRRC), Hsinchu, Taiwan, and the hard X-ray absorption data for the Pt L3-edge were collected at beamline BL17C. The acquired EXAFS raw data were then background-subtracted, normalized, and Fourier-transformed by using the ATHENA program in the IFEFFIT software package. Least-squares curve parameter fitting was performed using the ARTEMIS module of IFEFFIT software packages.

Electrochemical Measurements. All electrochemical tests were conducted on the CHI 760E workstation (CH Instruments, Inc.) with a RRDE-3A rotator (ALS Co., Ltd). A typical three-electrode system was employed, using a commercial glassy carbon (GC) electrode (3 mm diameter, 0.07065 cm^2) as the working electrode, a carbon rod and Ag/AgCl electrode (in saturated KCl solution) as the counter and reference electrodes, respectively. All potentials were referred to the reversible hydrogen electrode by adding a value of (0.197 + 0.059×pH) V. LSV with a scan rate of 10 mVs^{-1} was carried out from 0.2 to -0.7 V versus RHE in electrolyte solution under continuous purging with N_2. All

the electrochemical tests in this study were conducted at least three times to ensure the accuracy of the measurements.

Preparation of the working electrode. For the PtSA@BP electrode, different loading amounts of PtSA@BP on the GC electrodes were employed to record the LSV curves to optimize the test conditions. Typically, 1 mg of PtSA@BP and 50 μL of 5 wt % Nafion solution were dispersed in 950 mL of 4:1 v/v water/ethanol by sonication for 1 h to form a homogeneous solution. Then, 2.5 μL of the solution was loaded onto the GC electrode. The final loading of PtSA@BP on the GC electrodes was about 0.036 mg cm^{-2} with the Pt loading of 0.0009 mg_{Pt} cm^{-2}. By means of the above preparation procedure with 0.25, 0.5, 0.75, 2, and 3 mg of PtSA@BP instead of 1 mg of PtSA@BP, the working electrodes with PtSA@BP loading amounts of 0.009, 0.018, 0.027, 0.072, and 0.108 mg cm^{-2} (correspond to the Pt loading of 0.00023, 0.00045, 0.00068, 0.0018, and 0.0027 mg_{Pt} cm^{-2}) were also prepared. The LSV curves recorded on these PtSA@BP electrodes are shown in Figure S13. As can be seen, the overpotentials at a current density of 10 mA cm^{-2} decrease with the increase of the loading amount of Pt species in the range of 0.00023 to 0.0009 mg_{Pt} cm^{-2} and remain unchanged above 0.0009 mg_{Pt} cm^{-2}. As a result, the PtSA@BP electrode with the Pt loading amount of 0.0009 mg_{Pt} cm^{-2} (correspond to 0.036 mg cm^{-2} PtSA@BP loaded onto the GC electrode) was used to further investigate the HER activity of PtSA@BP. In addition, the working electrodes of PtSA@BP 0.4%, PtSA@BP 0.7%, and PtSA@BP 2.0% in the present work were also prepared by means of the above preparation procedure with 1 mg of PtSA@BP 0.4%, PtSA@BP 0.7%, and PtSA@BP 2.0% instead of 1 mg of PtSA@BP, respectively. It is worth noting that the

optimized loading amount of commercial Pt/C (20 wt%) on the GC electrode was also determined, which is ca. 0.229 mg cm^{-2} (correspond to the Pt loading of ca. 0.045 mg_{Pt} cm^{-2}). As for the working electrodes of original BP and NBP, 4 mg of sample and 50 μL of 5 wt % Nafion solution were dispersed in 950 mL of 4:1 v/v water/ethanol by sonication for 1 h to form a homogeneous solution. Then, 4 μL of the solution was loaded onto the GC electrode.

Determination of mass activity and turnover frequency (TOF). The mass activity and TOF can be calculated by the following equations.

$$mass\ activity = \frac{I}{m}$$

$$TOF = \frac{I}{2Fn}$$

Here, I is the current during the linear sweep measurement (in A); m is he catalyst loading; F is the Faraday constant (in C mol^{-1}); n is the number of actives sites (in mol). The factor 1/2 suggests that the formation of one hydrogen molecule needs two electrons.

Computational Methods. All spin-polarized first-principles calculations were performed by using the Perdew-Burke-Ernzerhof (PBE)[S2] exchange–correlation functional as implemented in the Vienna *ab initio* simulation package (VASP).[S3,S4] The projector augmented wave (PAW) pseudopotential was used and a cutoff energy of 500 eV was set for the plane wave basis set. DFT-D3 method was employed to describe the weak interactions in the systems.[S5] To avoid the interactions between slabs and their periodic images, a vacuum space of 15 Å was applied along the z-direction in the supercells. The

k-points of 2×2×1 were generated using the Monkhorst-Pack method. The convergence thresholds for the energy and force are 10^{-5} eV and 0.02 eV/Å, respectively.

To determine the stable adsorption site for the Pt atoms on graphene, the binding energy (E_b) for each site was calculated by the following equation:

$$E_b = (E_{nPt/NG-} - E_{NG} - nE_{Pt})/n$$

where $E_{nPt/NG-}$, E_{NG} and E_{Pt} represent the total energies of the Pt atoms embedded N-doped graphene, the N-doped graphene, and the isolated Pt atom, respectively. Accordingly, a more negative E_b value indicates that the adsorption of the Pt atoms on the N-doped graphene is thermodynamically more favorable.

The hydrogen adsorption Gibbs free energy is defined as:

$$\Delta G_{H^*} = \Delta E + \Delta ZPE - T\Delta S$$

where ΔE is the difference in electronic energies and defined as:

$$\Delta E = E_{H/surf} - E_{surf} - E_{H2}/2$$

where $E_{H/surf}$ and E_{surf} are the total energies of catalyst surface with and without the hydrogen atom, respectively, and E_{H2} means the energy of H_2 in gas phase. ΔZPE and ΔS are the changes in zero-point energy and entropy between the adsorbed and gas phase of hydrogen, respectively. In practice, the free energy can be approximately calculated as $\Delta G_{H^*} = \Delta E + 0.24$.[S6]

The adsorption energy of H_2O on catalyst surface was calculated as:

$$E_{ads} = E_{H2O/surf} - E_{surf} - E_{H2O}$$

where $E_{H2O/surf}$, E_{surf} and E_{H2O} are the total energies of the catalyst surface with and without adsorbed H_2O and an isolated H_2O molecule, respectively.

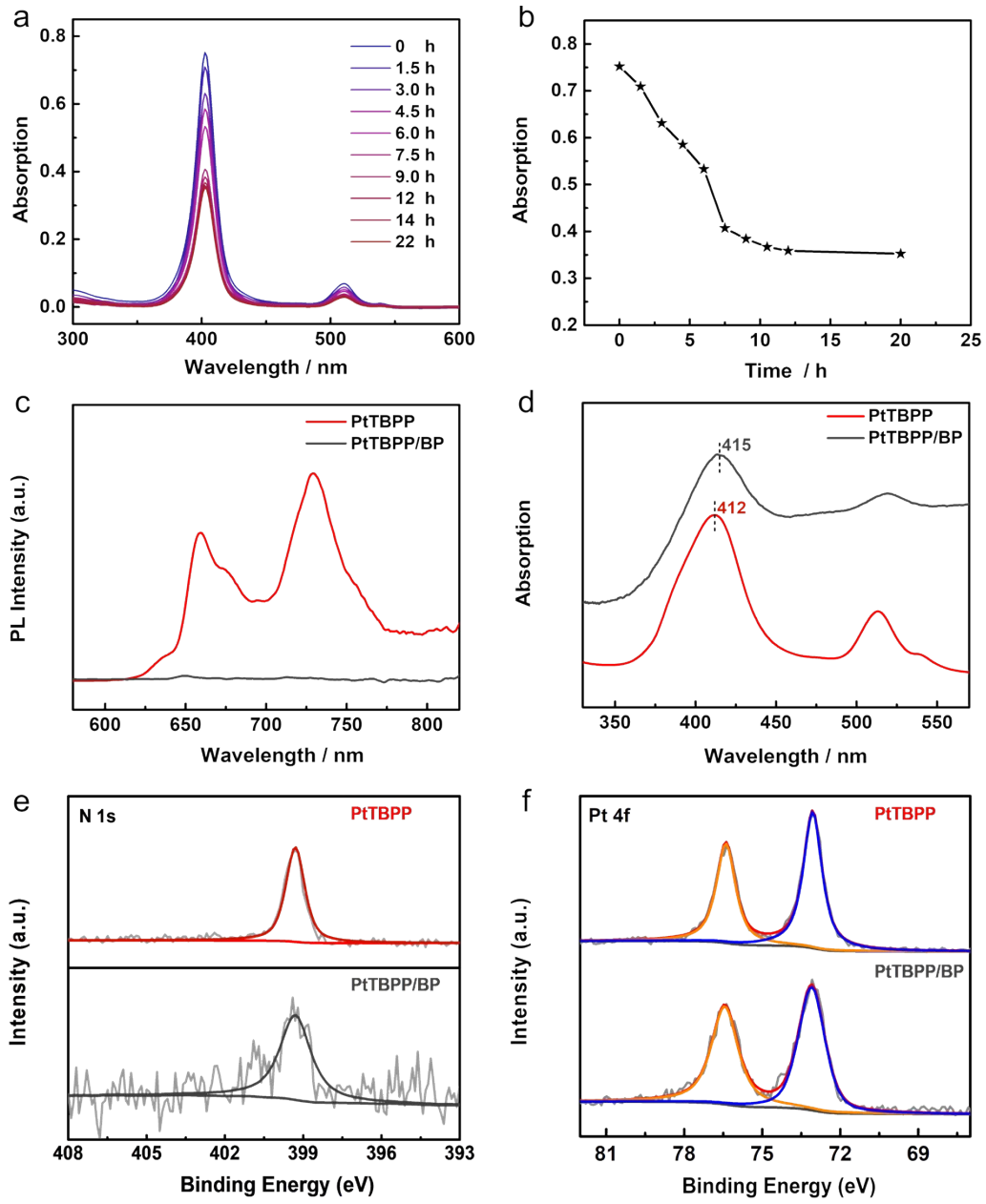

Fig. S1 (a) UV-vis absorpotion spectra of PtTBPP in THF at different times and (b) plot of absorption of PtTBPP in THF at 401 nm as a function of time during the preparation of PtTBPP/BP. (c) Solid-state fluorescence spectra PtTBPP and PtTBPP/BP. (d) Solid-state UV-vis diffuse reflectance spectra of PtTBPP and PtTBPP/BP. XPS high resolution (e) N 1s and (f) Pt 4f spectra of PtTBPP and PtTBPP/BP.

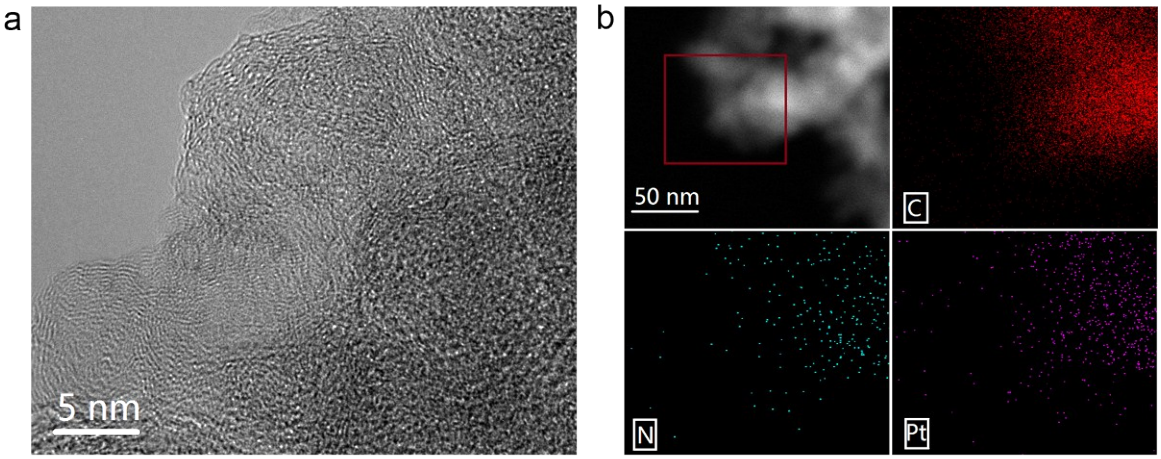

Fig. S2 (a) HRTEM image and STEM-EDS element mapping of PtTBPP/BP.

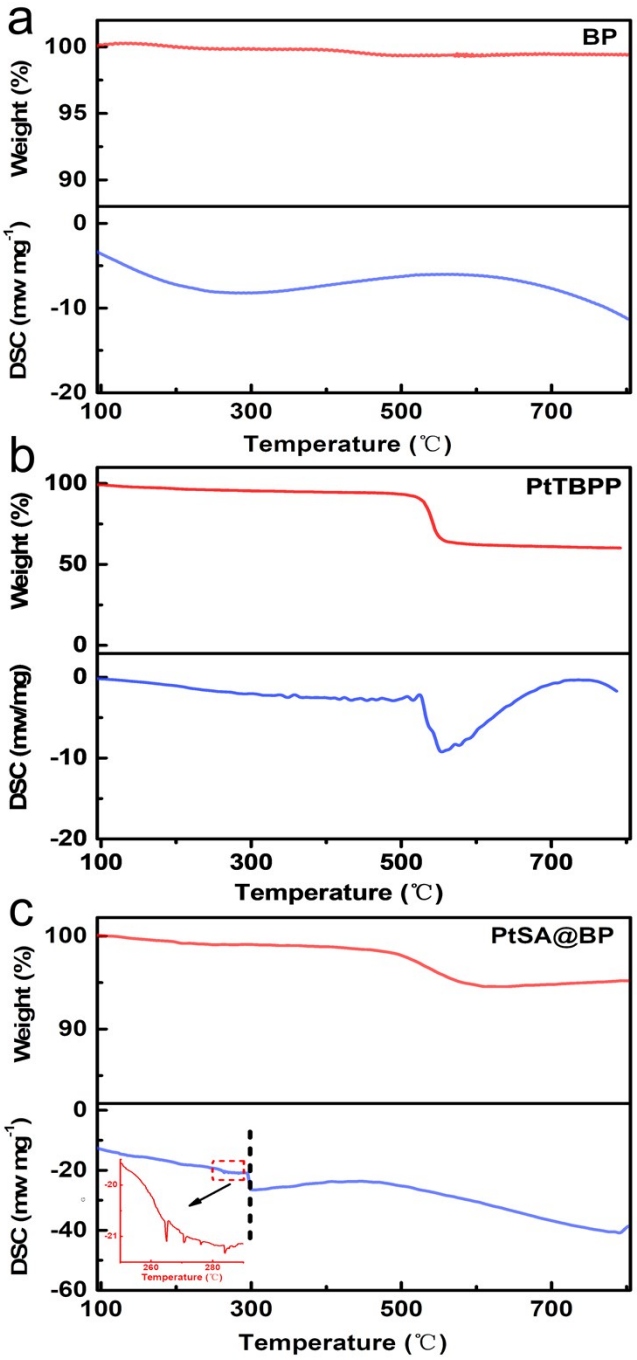

Fig. S3 TG and DSC of (a) PtTBPP, (b) BP, and (c) PtTBPP/BP (the left side of the dashed line is tested in the differential thermal instrument).

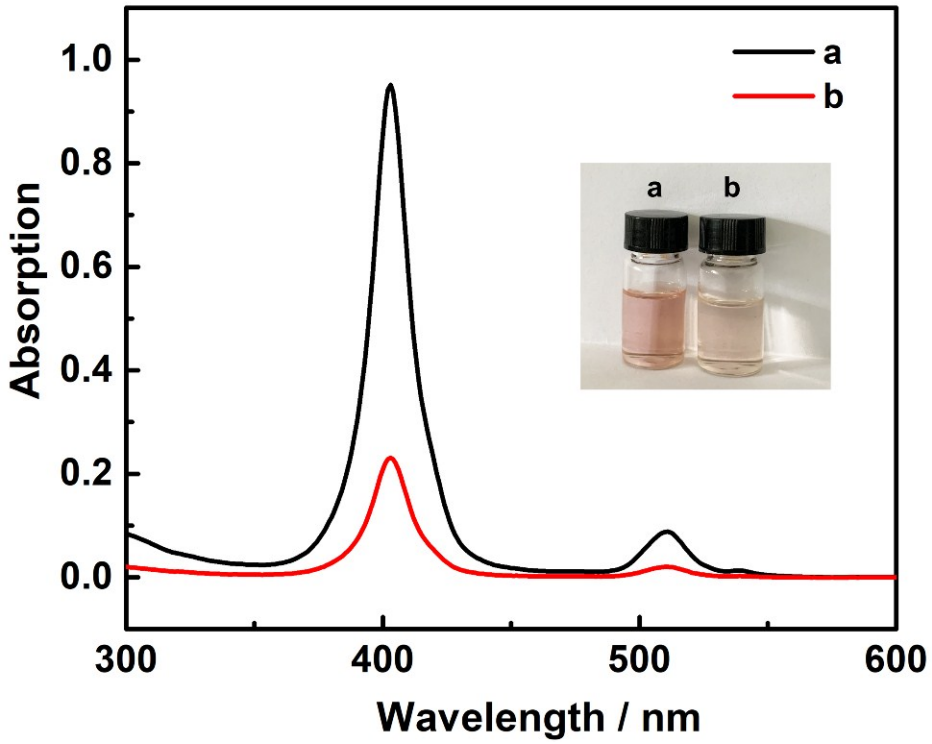

Fig. S4 UV-vis absorpotion spectra and images of immersing the (a) original PtTBPP/BP hybrid and (b) PtTBPP/BP hybrid after heating at 280°C for 1 h into THF.

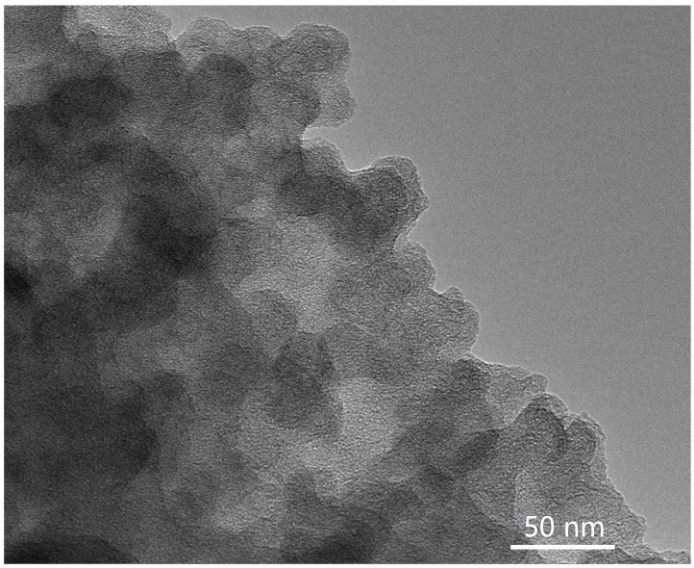

Fig. S5 The TEM image of BP.

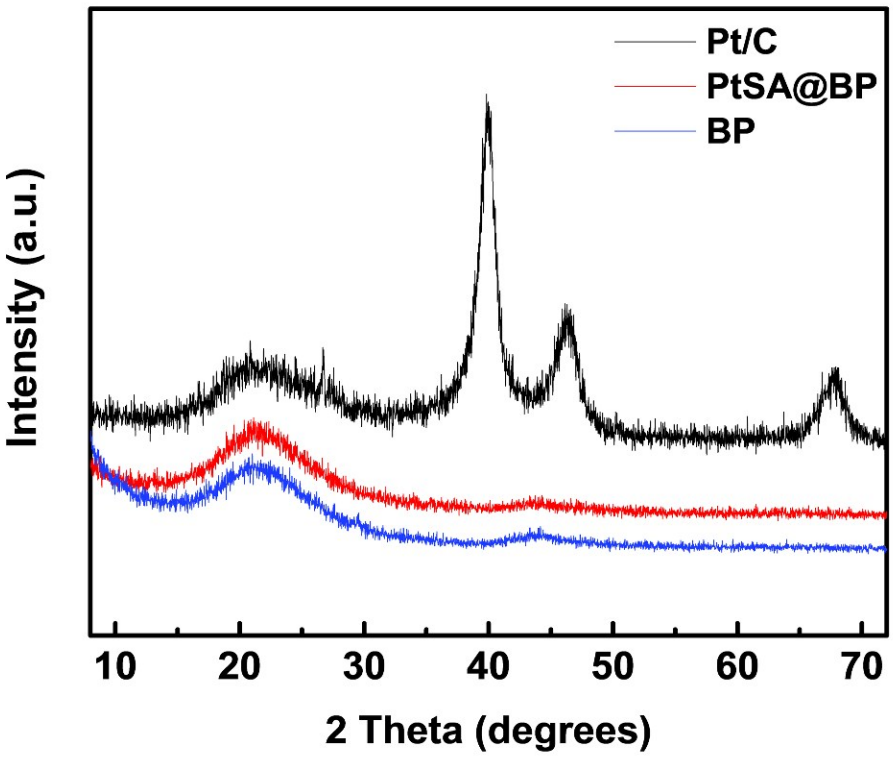

Fig. S6 PXRD patterns of Pt/C, PtSA@BP, and BP.

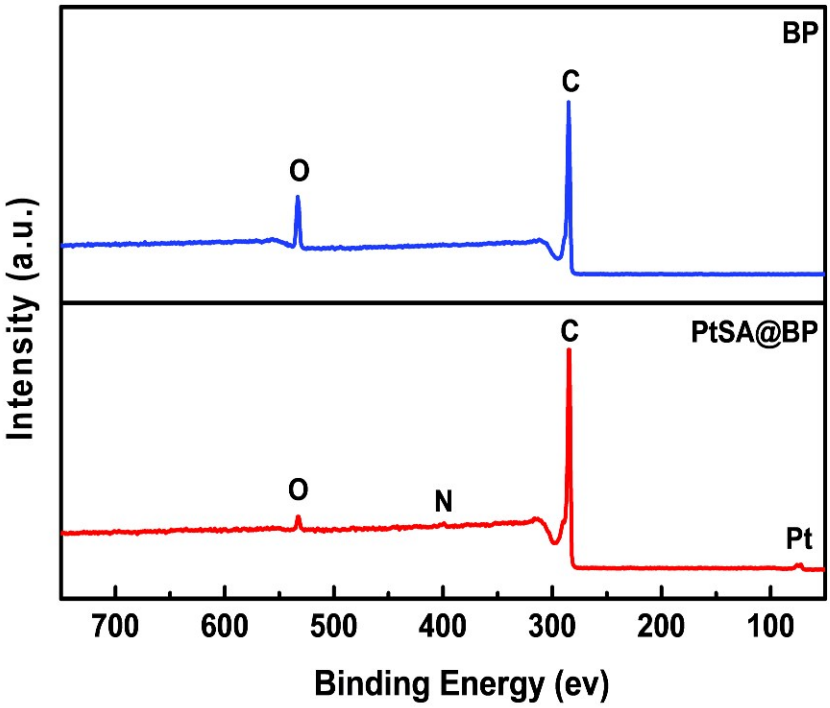

Fig. S7 XPS overall spectra of BP and PtSA@BP.

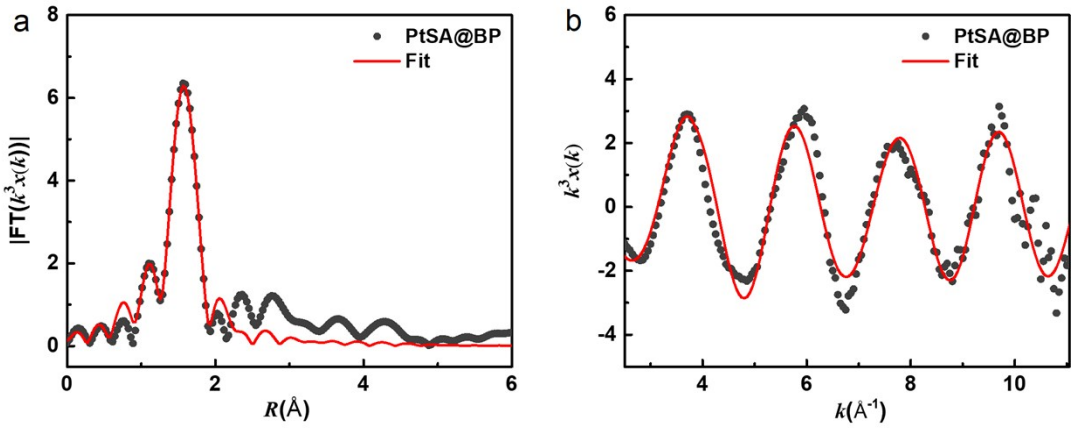

Fig. S8 EXAFS fitting curves of the PtSA@BP in (a) R- and (b) k-space. In the EXAFS fitting, the amplitude reduction factor S_0^2 (0.80) was fixed, while the number of neighbors N, internal atomic distances R, Debye-Waller factor σ^2, and the edge-energy shift ΔE_0 were allowed to run freely. Two scattering paths (Pt-N and Pt-C) were applied. (the obtained coordination number of Pt-N and Pt-C was 1.1 and 2.4, respectively).

Fitting results of Pt L3-edge EXAFS curves.

Sample	Scattering pair	N	R(Å)	$\sigma^2(10^{-3}$ Å$^2)$	ΔE_0(eV)	R factor
Pt foil	Pt-Pt	12.0	2.77			
PtO_2	Pt-O	6.0	2.07			
PtSA@BP	Pt-C	2.4	1.97	0.1	12.57	0.0016
	Pt-N	1.1	2.12	0.1	12.57	

N is the coordination number; R is interatomic distance (the bond length between central atoms and surrounding coordination atoms); σ^2 is Debye-Waller factor (a measure of thermal and static disorder in absorber-scatterer distances); ΔE_0 is edge-energy shift. R factor is used to value the goodness of the fitting.

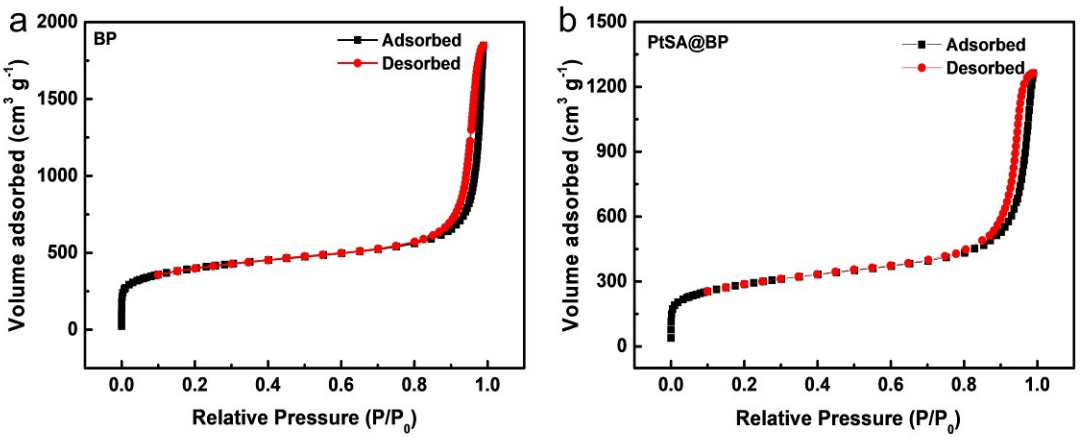

Fig. S9 N_2 sorption isotherms of (a) BP and (b) PtSA@BP at 77K.

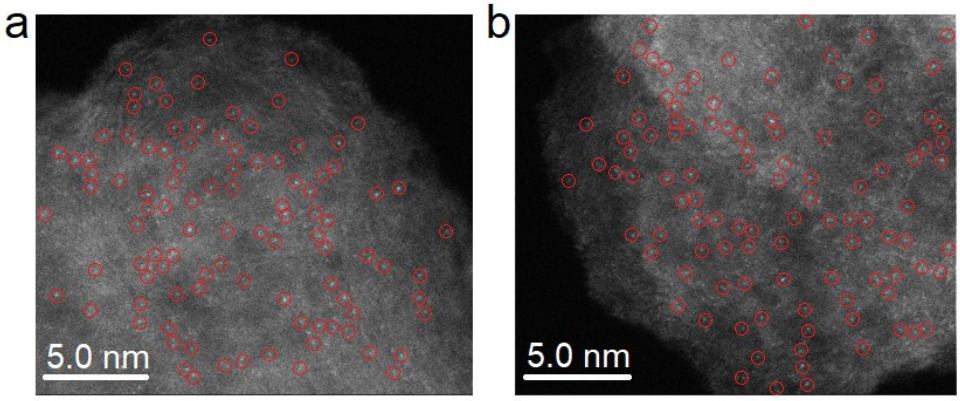

Fig. S10 The aberration-corrected HAADF-STEM images of (a) PdSA@BPand (b) RhSA@BP.

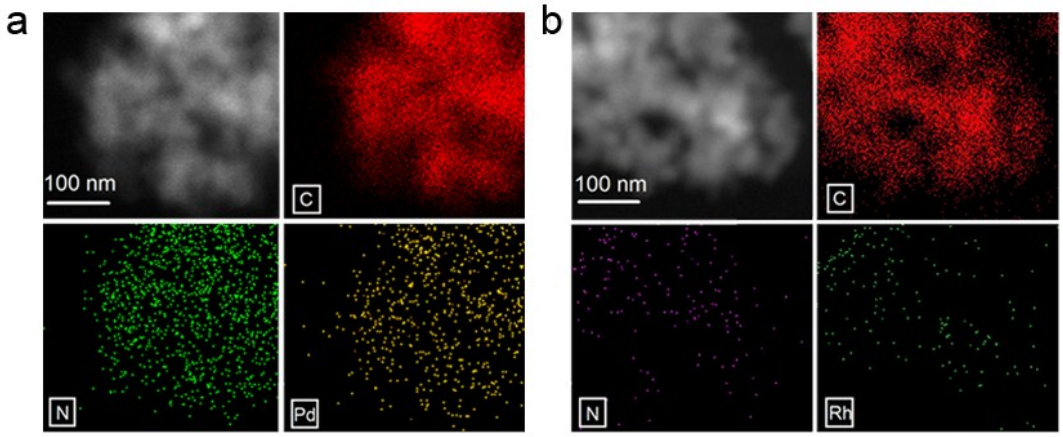

Fig. S11 The HAADF-STEM and EDS element mapping images (a) of PdSA@BP and (b) RhSA@BP.

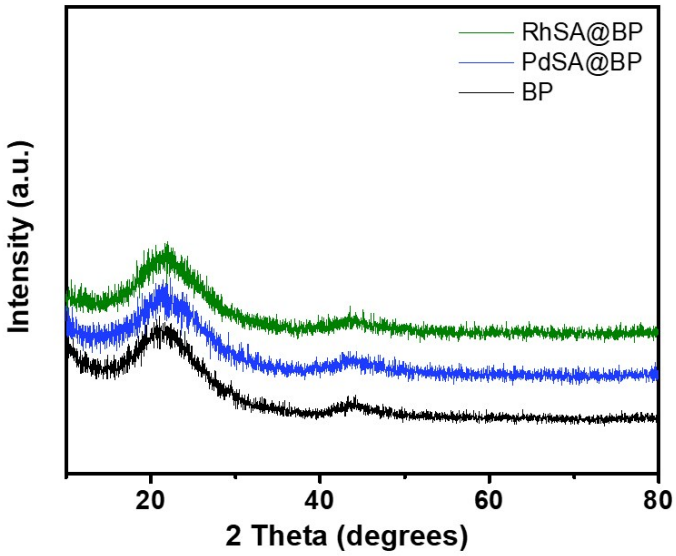

Fig. S12. PXRD patterns of RhSA@BP, PdSA@BP, and BP.

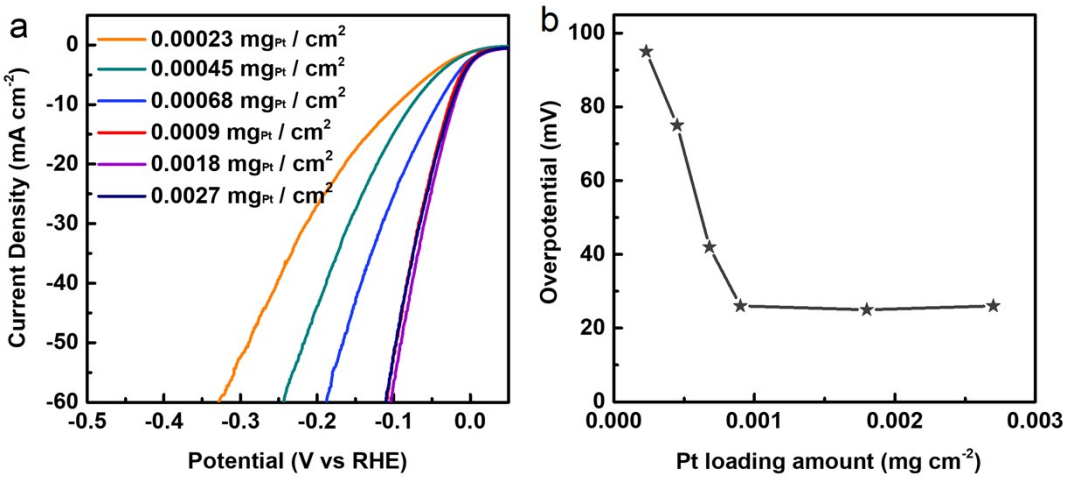

Fig. S13 (a) LSV curves on the PtSA@BP electrodes with the different loading amounts of Pt species in 1.0 M KOH at a scan rate of 5 mV s^{-1}. (b) The overpotential at a current density of 10 mA cm^{-2} on PtSA@BP electrodes with the different loading amounts of Pt species.

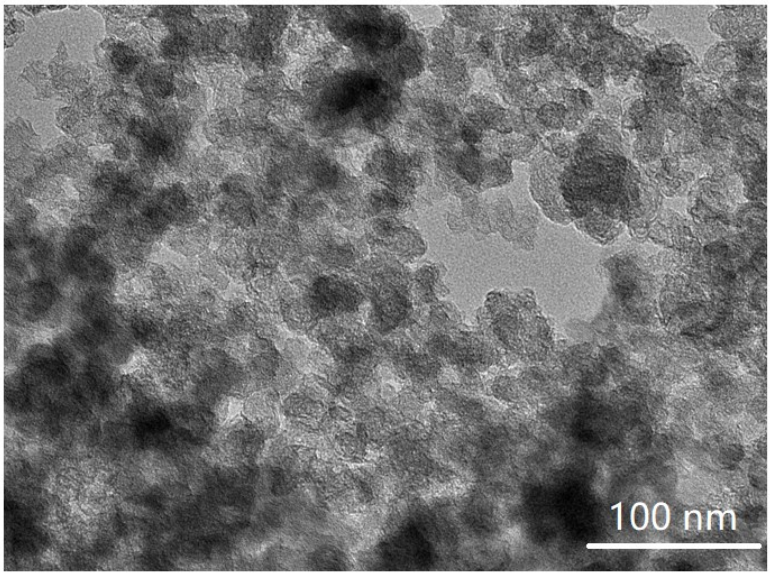

Fig. S14. TEM image of PtSA@BP after i-t test.

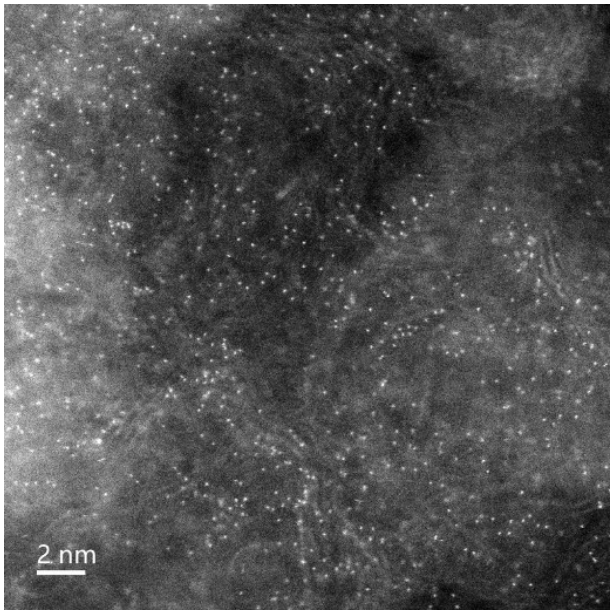

Fig. S15. The aberration-corrected HAADF-STEM image of PtSA@BP after i-t test.

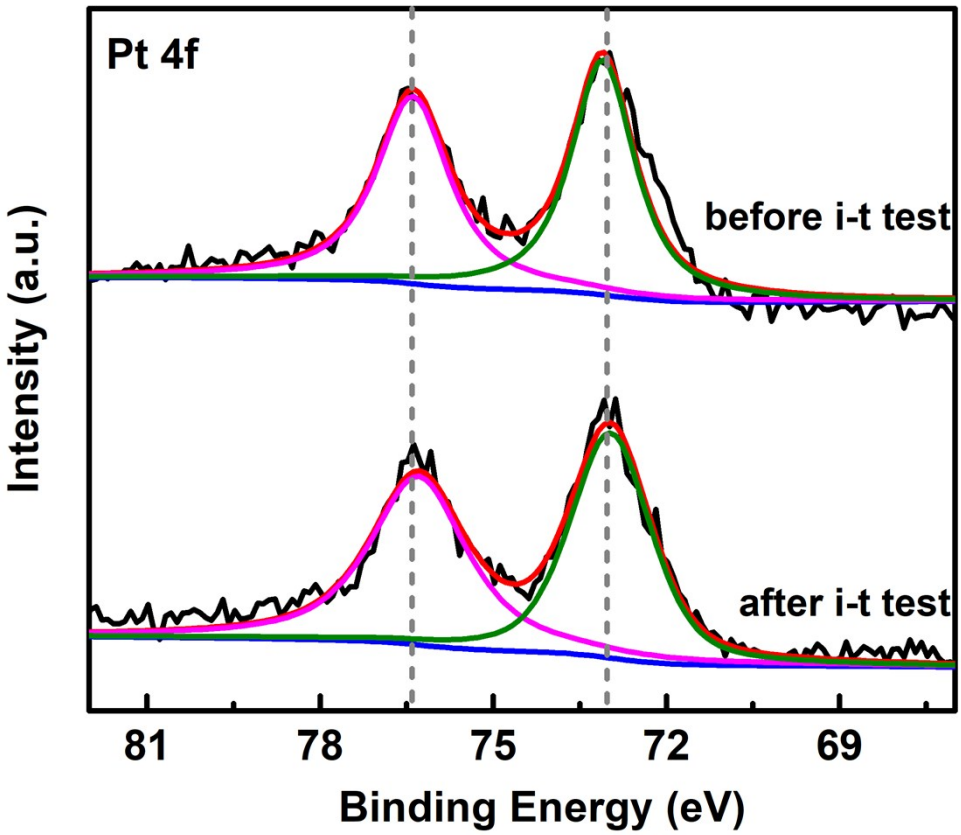

Fig. S16 XPS high resolution Pt 4f spectra of PtSA@BP before and after i-t test.

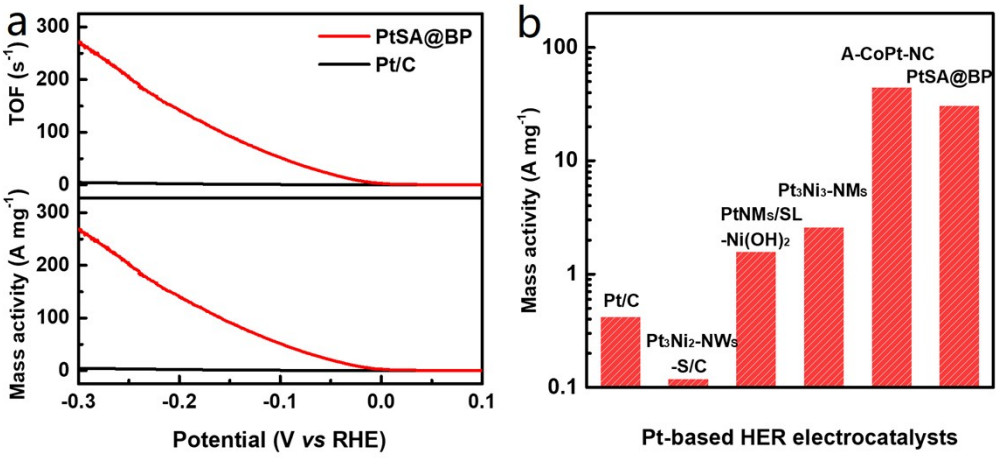

Fig. S17 (a) TOFs (top) and mass activities (bottom) of PtSA@BP and Pt/C at varied overpotentials in 1.0 M KOH. (b) Mass activity of various Pt-based HER electrocatalysts at an overpotential of 70 mV in alkaline media.

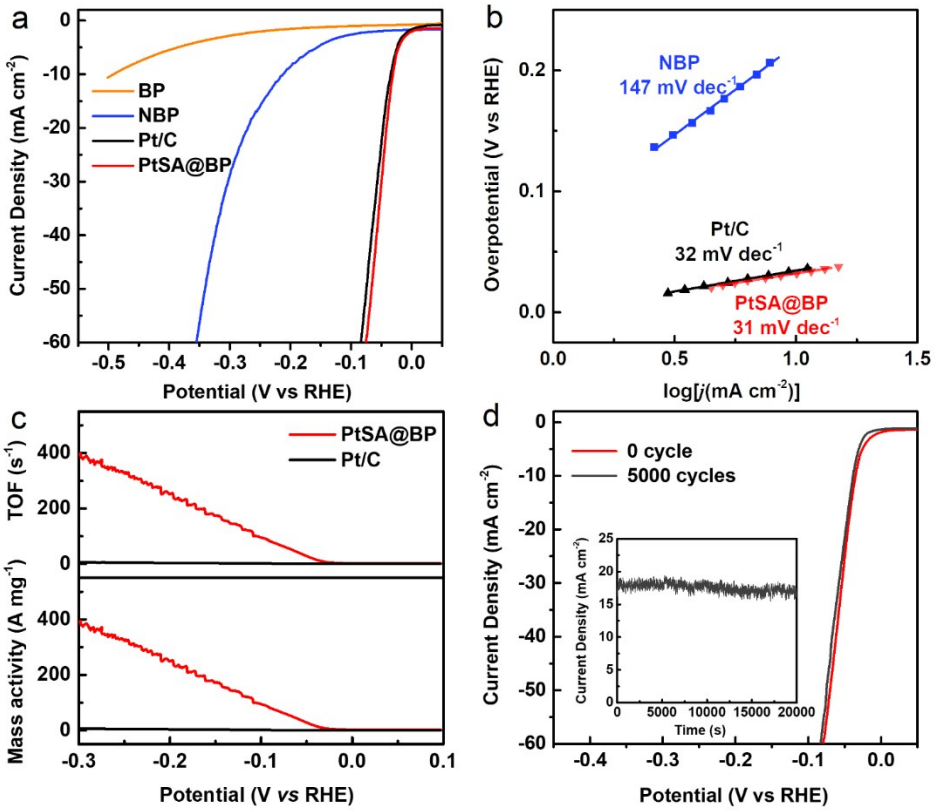

Fig. S18 (a) LSV curves of BP, NBP, PtSA@BP, and Pt/C in 0.5 M H_2SO_4 at a scan rate of 5 mV s^{-1}. (b) Tofel plots of NBP, PtSA@BP, and Pt/C in 0.5 M H_2SO_4. (c) TOFs (top) and mass activities (bottom) of PtSA@BP and Pt/C at varied overpotentials in 0.5 M H_2SO_4. (d) Polarization curves of PtSA@BP recorded initially and after 5000 cyclic voltammetry scans at a scan rate of 50 mV s^{-1}. Inset shows the chronoamperometric responses recorded on PtSA@BP for 20000s.

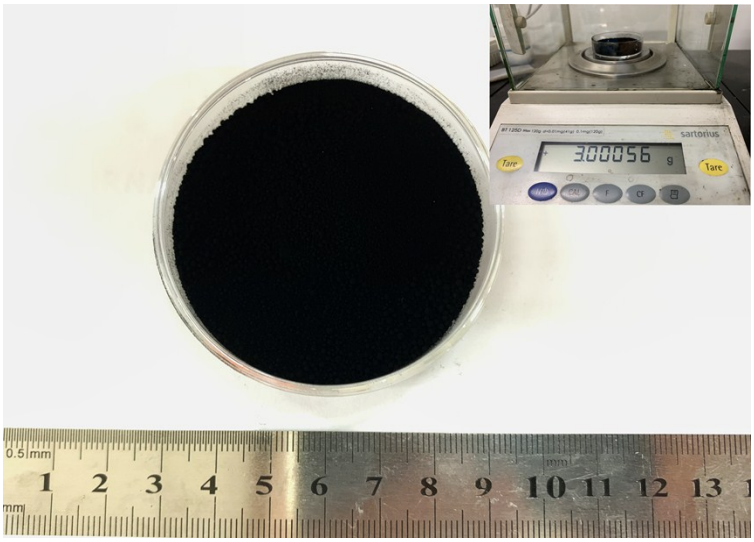

Fig. S19 Picture of ~3000 mg of the PtSA@BP catalyst.

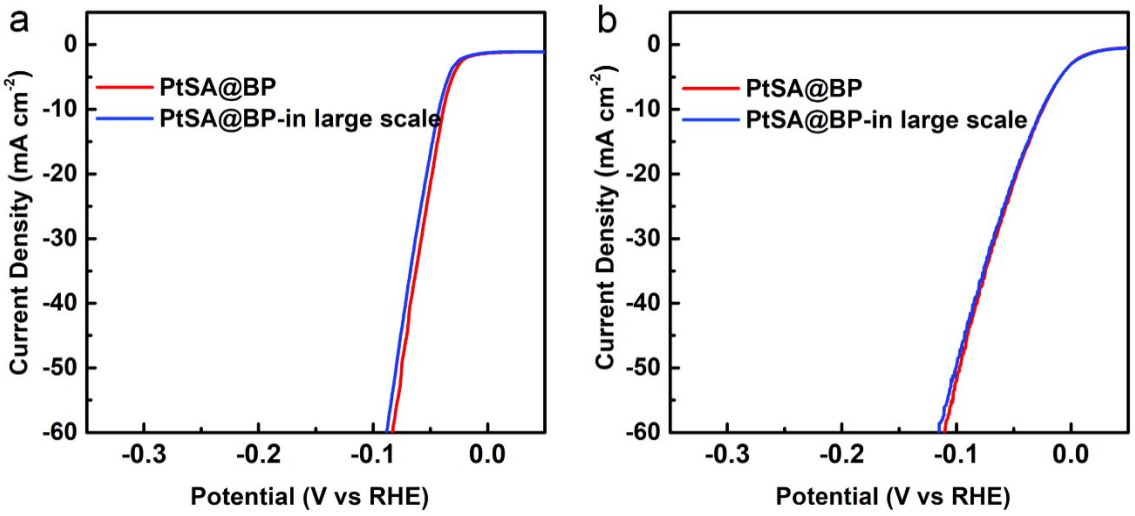

Fig. S20 LSV curves of PtSA@BP and PtSA@BP-in large scale in (a) 0.5 M H_2SO_4 and (b) 1.0 M KOH.

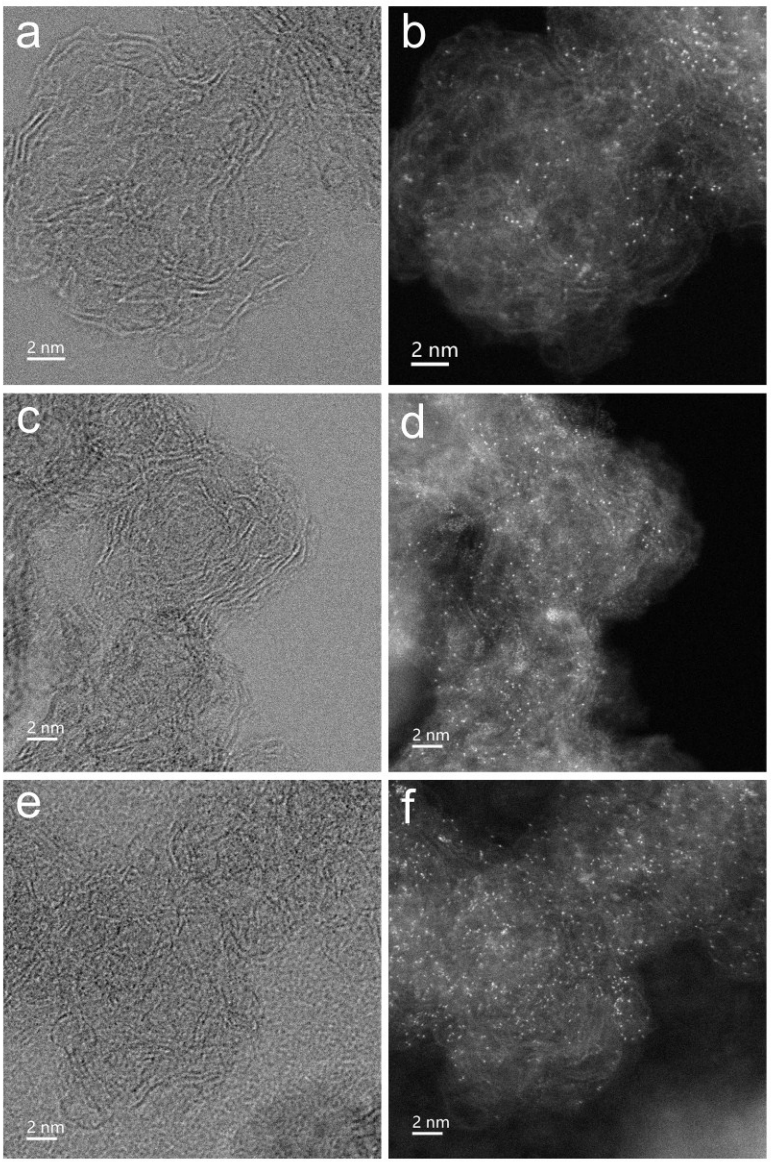

Fig. S21 The HRTEM images and aberration-corrected HAADF-STEM images of (a)(b) PtSA@BP 0.4%, (c)(d) PtSA@BP 0.7%, and (e)(f) PtSA@BP 2.0%.

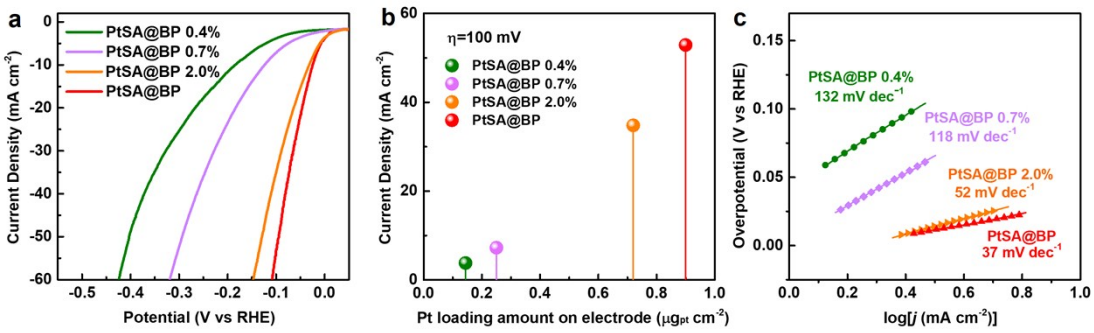

Fig. S22 (a) LSV curves of PtSA@BP 0.4%, PtSA@BP 0.7%, PtSA@BP 2.0%, and PtSA@BP in 1.0 M KOH at a scan rate of 5 mV s^{-1}. (b) Comparison of the current densities of PtSA@BP 0.4%, PtSA@BP 0.7%, PtSA@BP 2.0%, and PtSA@BP at an overpotential of 100 mV in 1.0 M KOH.(c) Tofel plots of PtSA@BP 0.4%, PtSA@BP 0.7%, PtSA@BP 2.0%, and PtSA@BP in 1.0 M KOH.

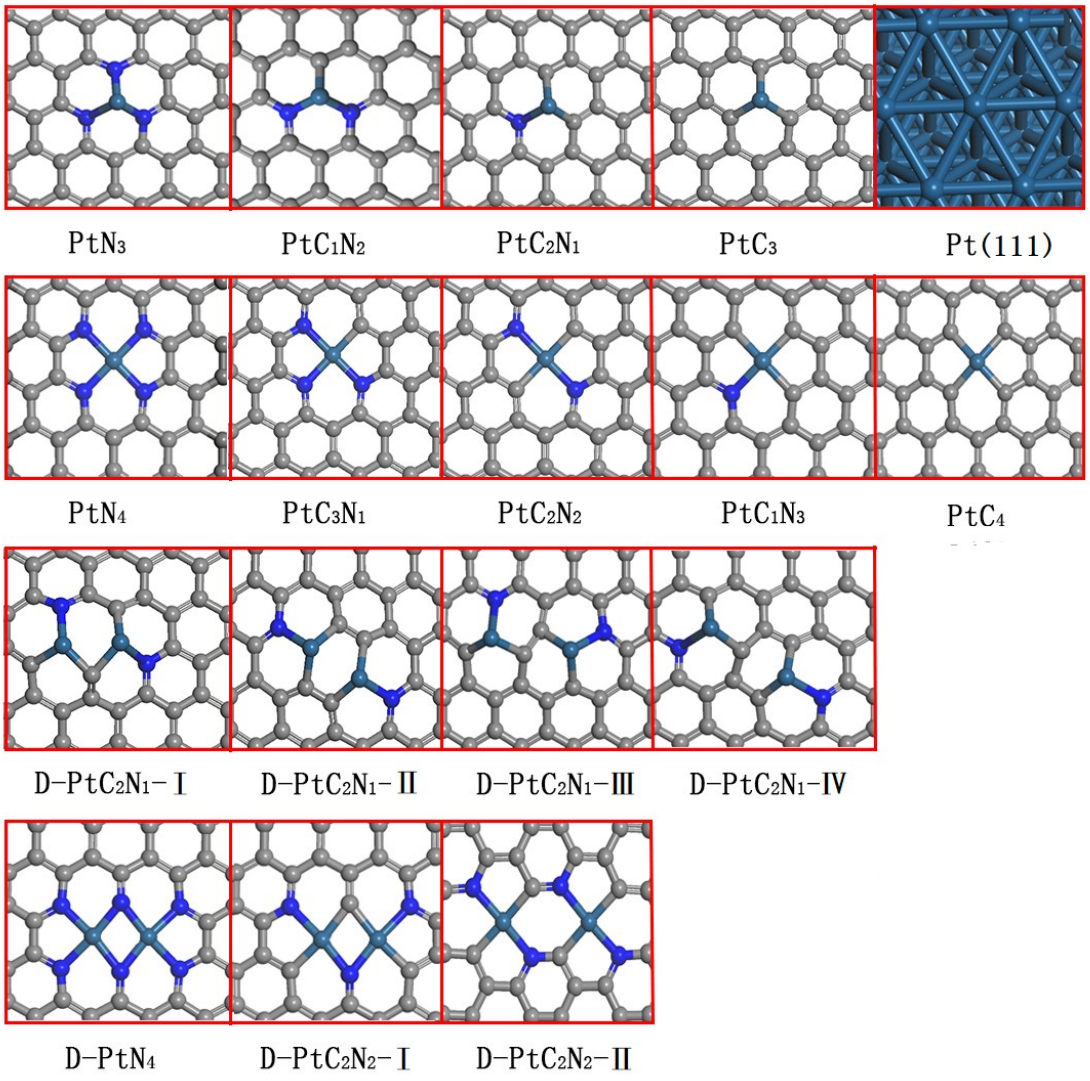

Fig. S23 Optimized structures of Pt atoms embedded into different types of N-graphene. The gray, blue, and green spheres represent C, N, and Pt atoms, respectively.

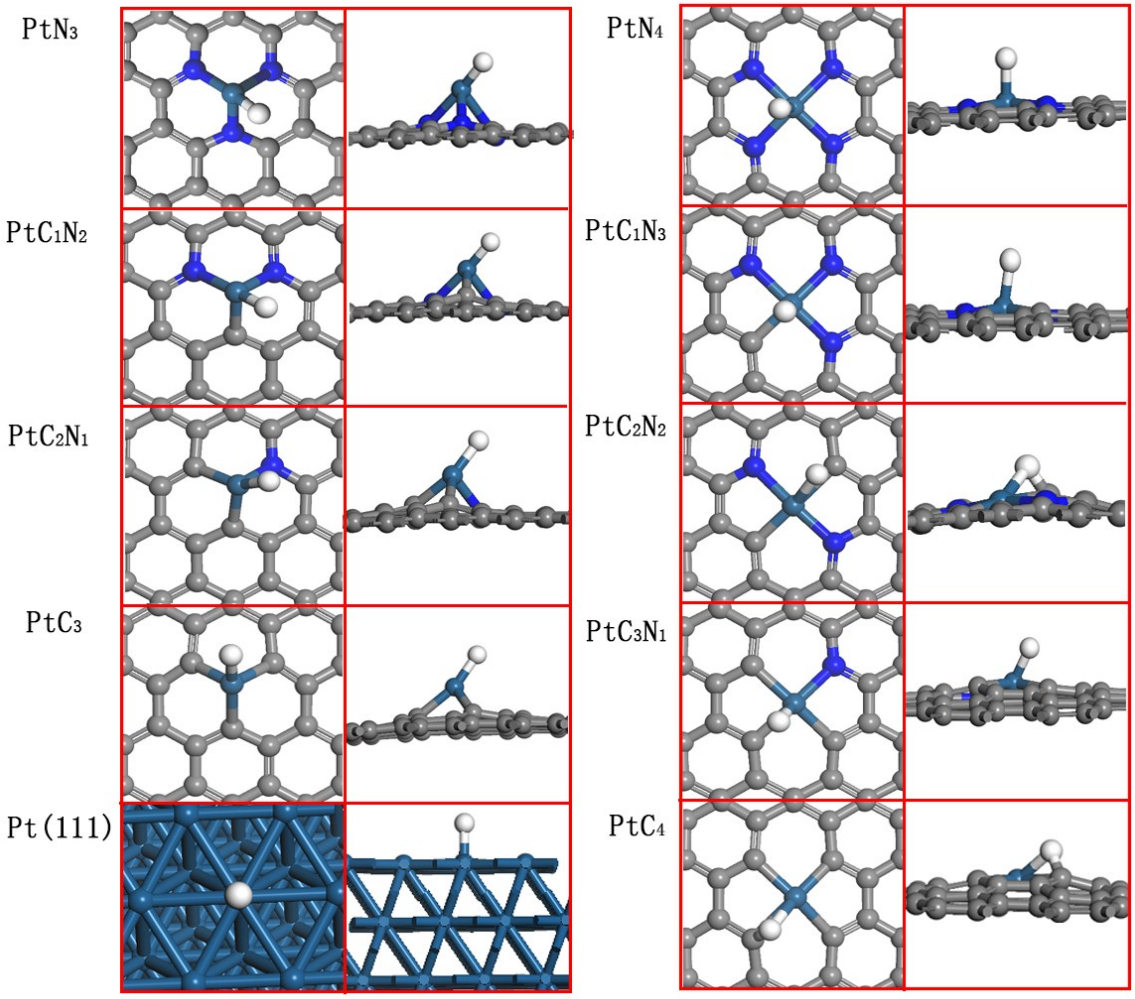

Fig. S24 Top and side views of the stable configurations of H adsorbed on the Pt atoms of single-atomic PtC_xN_y moieties and Pt (111). The gray, blue, green, and white spheres represent C, N, Pt, and H atoms, respectively.

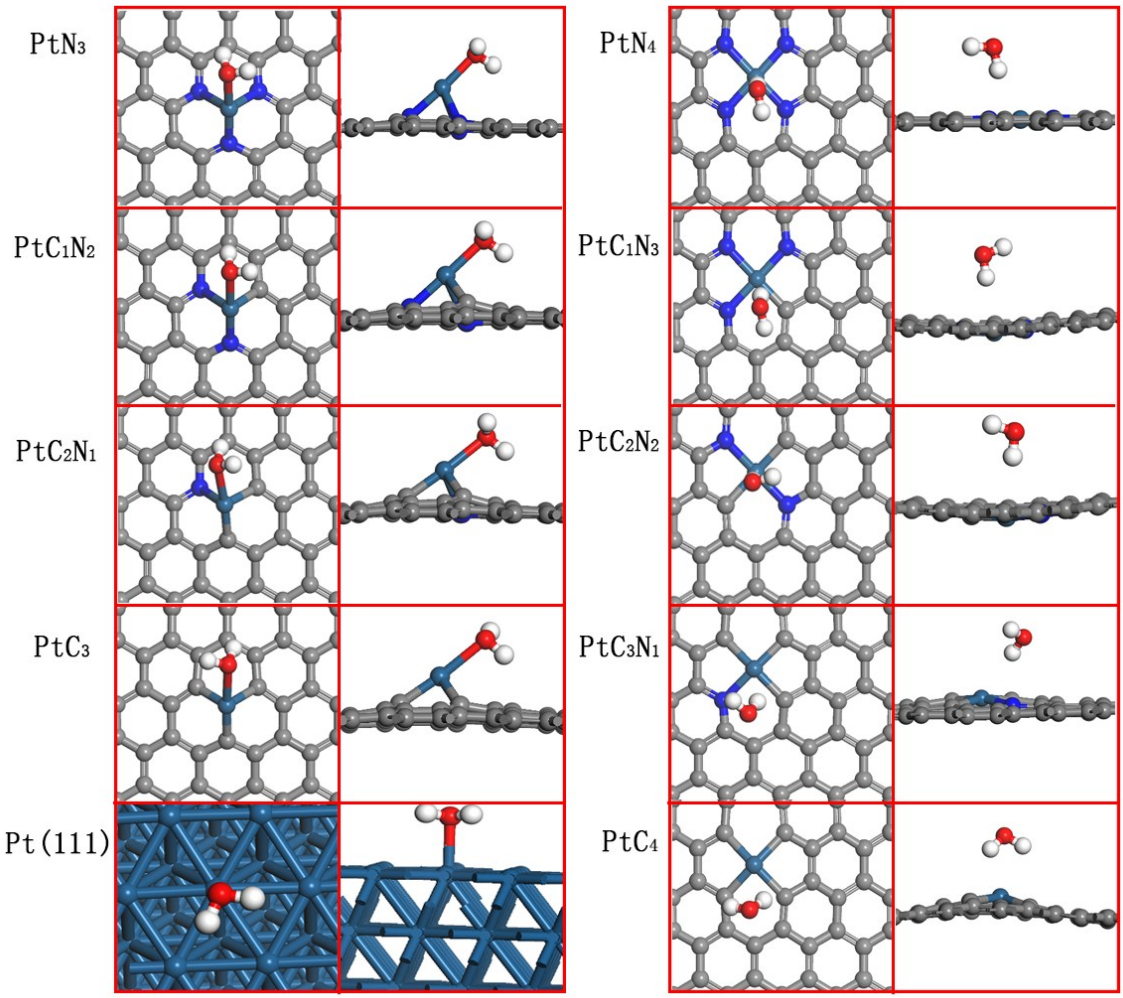

Fig. S25 Top and side views of the stable configurations of H_2O molecule adsorbed on the Pt atoms of single-atomic PtC_xN_y moieties and Pt (111). The gray, blue, green, red, and white spheres represent C, N, Pt, O, and H atoms, respectively.

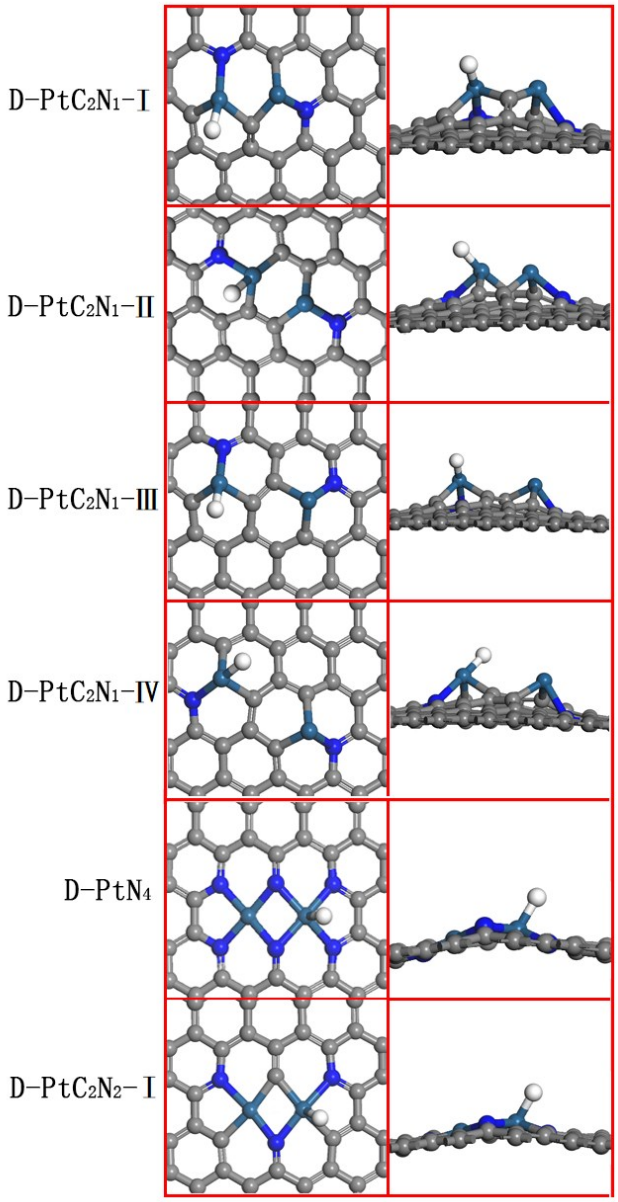

Fig. S26 Top and side views of the stable configurations of H adsorbed on the Pt atoms of the structures containing two PtC_xN_y moieties. The gray, blue, green, and white spheres represent C, N, Pt, and H atoms, respectively.

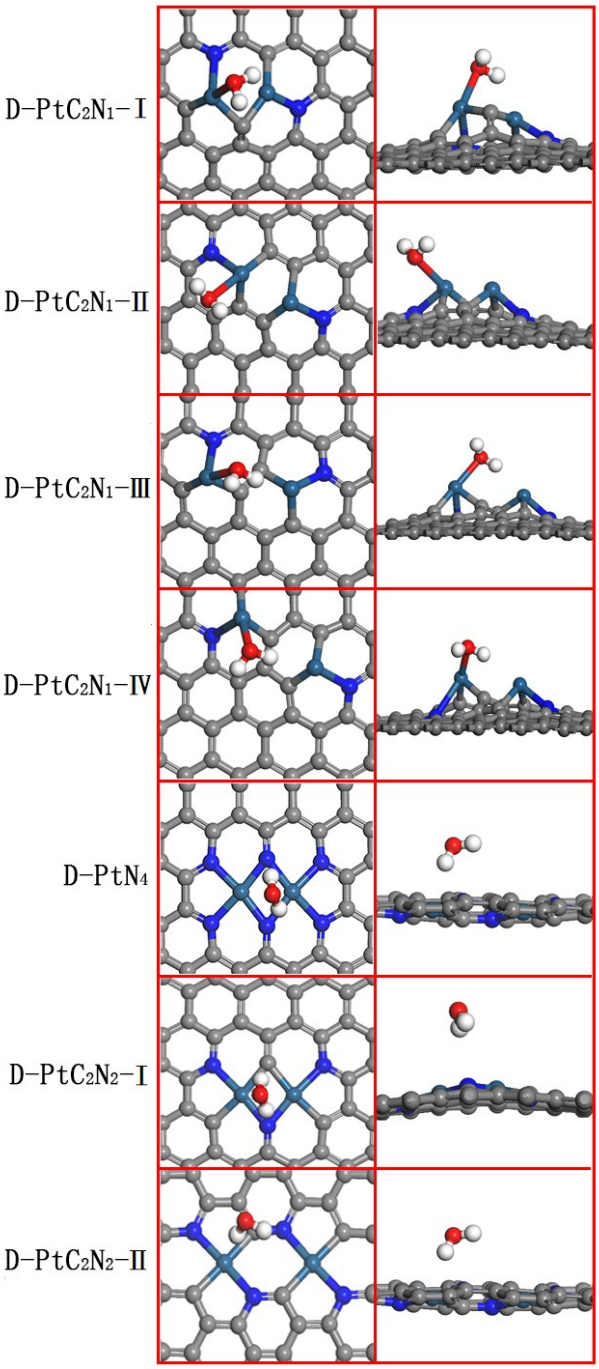

Fig. S27 Top and side views of the stable configurations of H_2O molecule adsorbed on the Pt atoms of the structures containing two PtC_xN_y moieties. The gray, blue, green, red, and white spheres represent C, N, Pt, O, and H atoms, respectively.

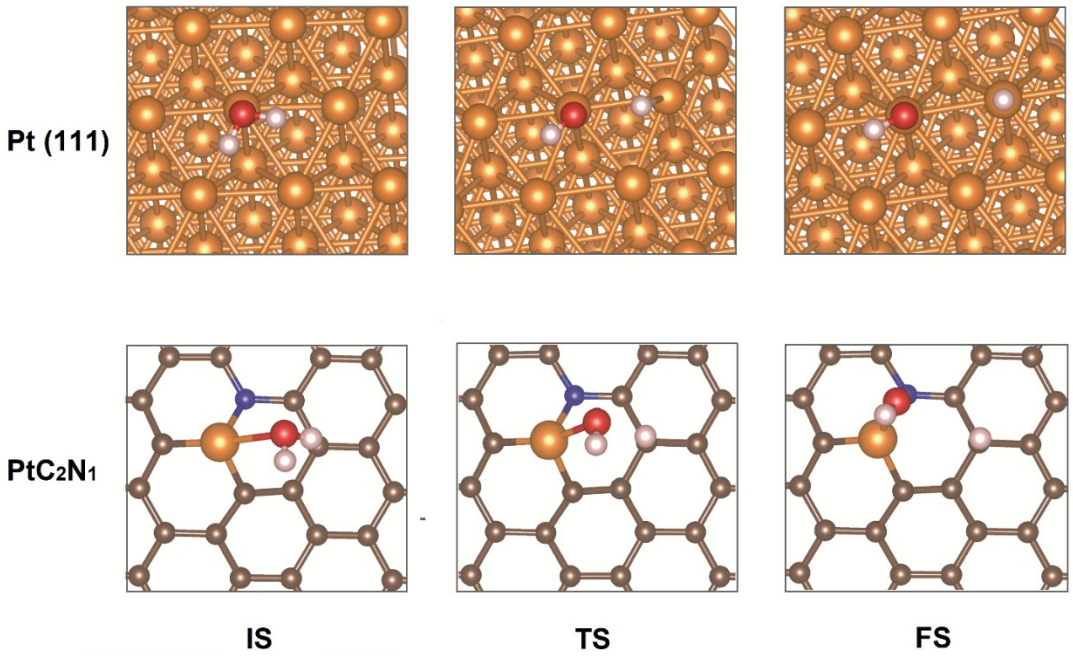

Fig. S28 The structures of initial state (IS), the transtion state (TS), and final state (FS) for Pt (111) and PtC_2N_1. The brown, golden, blue, red, and white spheres represent C, Pt, N, O, and H atoms, respectively

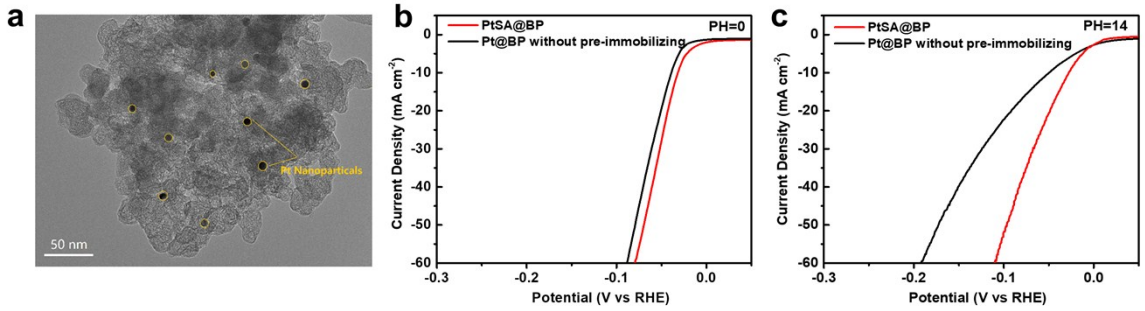

Fig. S29 (a) TEM image of Pt@BP without pre-immobilizing. LSV curves of PtSA@BP and Pt@BP without pre-immobilizing in (b) 0.5 M H_2SO_4 and (c) 1.0 M KOH. Pt@BP without pre-immobilizing refers to direct heating of PtTBPP/BP hybrid at 800°C for 2 h without pre-heating at 280°C.

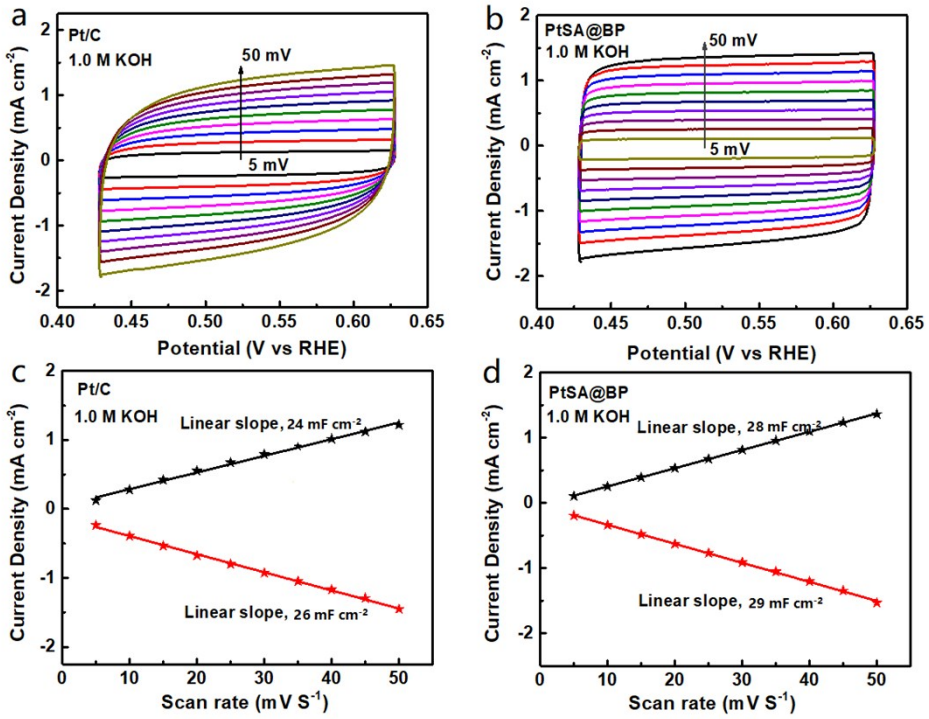

Fig. S30 (a)(b) CV conducted at potential from 0.43 V to 0.63 V *vs* RHE at scan rates of 5 mV $s^{-1}$to 50 mV s^{-1} in 1.0 M KOH. (c)(d) The current densities of anode and cathode measured at 0.52 V *vs* RHE with different scan rates. (a)(c) and (b)(d) are Pt/C and PtSA@BP, respectively.

To study the electrochemically active surface area (ECSA) of Pt/C and PtSA@BP. we conducted the CV cycles at different scan rates during the potential from 0.43 V to 0.63 V *vs* RHE in 1.0 M KOH, where there is no Faradic current. At last, the ECSA was estimated from the as obtained double-layer capacitance (C_{dl}). According to C_{dl} is constant, it can be calculated as:

$$C_{dl} = Q/U = (dQ/dt)/(dU/dt) = j/r,$$

Q is the quantity of electric charge per unit area,

U is the voltage,

j is the current density and

r is the scan rate

From Eq, the C_{dl} is the slope of *j*~*r*, which can be obtained by the Fig. S30c and S30d. The average Cdl of Pt/C and PtSA@BP are 25 mF/cm^2, and 29 mF/cm^2, respectively. The ECSA can be calculated as:

$$ECSA = C_{dl}/C_s$$

C_s is the specific capacitance value for a flat standard with 1 cm^2 of real surface area. The general value for C_s is between 20 μF/cm^2 and 60 μF/cm^2. Here we use 40 μF/cm^2 as the average value (*Nat. Commun.* **2015***, 6,* 8668). Thus the ECSA for Pt/C and PtSA@BP can be obtained as 625 cm^2 and 725 cm^2. respectively.

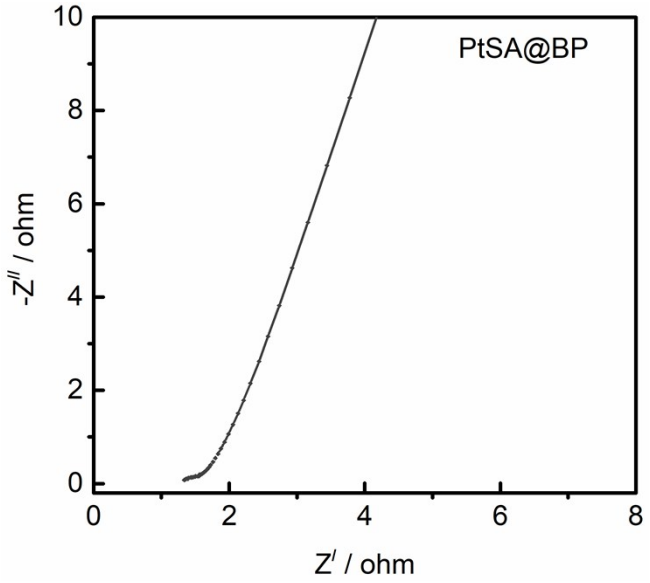

Fig. S31. Impedance curve of PtSA@BP.

Table S1. Comparison of Pt loading amount (wt %) in recent literatures.

Catalyst	Pt loading amount (wt %)	References
Pt@PCM	0.53	(S7)
Pt_1-N/BP	0.4	(S8)
A-CoPt-NC	0.16	(S9)
PtSAs/DG	2.1	(S10)
PtSA@BP	2.5	This work
PtSA@BP 0.4%	0.4	This work
PtSA@BP 0.7%	0.7	This work
PtSA@BP 2.0%	2.0	This work

Table S2. Summary of representative HER catalysts in acidic and Alkaline electrolyte**.**

Catalyst	Electrolyte	Overpotential (10mA cm^{-2})	Tafel slope	References
Pt@PCM	1.0 M KOH	139	63.7	(S7)
Ni_3N/Pt	1.0 M KOH	50	36.5	(S8)
Pd-Pt-T	1.0 M KOH	70	45	(S9)
er-WS_2-Pt	1.0 M KOH	65	60	(S10)
Mo_2C@NC@Pt	1.0 M KOH	47	57	(S11)
$Pt_{75}Mo_{25}$@graphene	1.0 M KOH	97	51	(S12)
$Ni(OH)_2$-Pt_2NS/Ti	1.0 M KOH	66.7	89	(S13)
Ru/NC	1.0 M KOH	21	31	(S14)
$Mo_1N_1C_2$	0.1 M KOH	132	90	(S15)
Ni_{SA}-MoS_2	1.0 M KOH	95	75	(S16)
Co_1/PCN	1.0 M KOH	89	52	(S17)
PtSA@BP	1.0 M KOH	26	37	This work
Pt@PCM	0.5 M H_2SO_4	105	65.3	(S7)
$PtSA_S$/DG	0.5 M H_2SO_4	23	25	(S18)
RuSAs@PN	0.5 M H_2SO_4	24	38	(S19)
Pt_1/OLC	0.5 M H_2SO_4	38	36	(S20)
er-WS_2-Pt	0.5 M H_2SO_4	40	27	(S10)
Cu@MoS_2	0.5 M H_2SO_4	131	51	(S21)
Co-SAC	0.5 M H_2SO_4	230	99	(S22)
PtSA@BP	0.5 M H_2SO_4	31	31	This work

Table S3. Calculated Pt binding energies (E_b), hydrogen adsorption Gibbs free energies (ΔG_{H*}), and H_2O adsorption energies (E_{ads}) on the different models of Pt-embedded N-doped graphene.

species	E_b/eV	ΔG_{H*}/eV	E_{ads}/eV	Pt-Pt distance (Å)
PtN_4	-7.99	0.15	-0.25	-
PtC_1N_3	-8.89	0.20	-0.22	-
PtC_2N_2	-9.68	-0.06	-0.30	-
PtC_3N_1	-8.45	-0.27	-0.26	-
PtC_4	-7.83	-0.36	-0.23	-
PtN_3	-2.747	-0.87	-0.71	-
PtC_1N_2	-4.87	-0.42	-0.86	-
PtC_2N_1	-5.22	-0.16	-1.02	-
PtC_3	-6.64	-0.20	-0.53	-
D-PtC_2N_1- Ⅰ	-5.7	-0.78	-0.79	2.57
D-PtC_2N_1- Ⅱ	-6.15	-0.48	-0.63	2.63
D-PtC_2N_1-Ⅲ	-5.62	-0.17	-1.14	3.82
D-PtC_2N_1-Ⅳ	-4.86	-0.33	-1.09	4.04
D-PtN_4	-8.12	-0.13	-0.18	2.67
D-PtC_2N_2- Ⅰ	-9.05	-0.13	-0.2	2.41
D-PtC_2N_2- Ⅱ	-9.76	-	-0.23	4.20
Pt (111)	-	-0.11	-0.50	-

References

(S1) K. T. Weber, K. Karikis, M. D. Weber, P. B. Coto, A. Charisiadis, D. Charitaki, G. Charalambidis, P. Angaridis, A. G. Coutsolelos and R. D. Costa, *Dalton Trans.*, 2016, **45**, 13284-13288.

(S2) J. P. Perdew, K. Burke and M. Ernzerhof, *Phys. Rev. Lett.*, 1996, **77**, 3865-3868.

(S3) G. Kresse and J. Hafner, *Phys. Rev. B*, 1993, **48**, 13115-13118.

(S4) G. Kresse and J. Furthmüller, *Phys. Rev. B*, 1996, **54**, 11169-11186.

(S5) S. Grimme, S. Ehrlich and L. Goerigk, *J. Comput. Chem.*, 2011, **32**, 1456-1465.

(S6) J. K. Nørskov, T. Bligaard, A. Logadottir, J. R. Kitchin, J. G. Chen, S. Pandelov and U. Stimming, *J. Electrochem. Soc.*, 2005, **152**, J23-J26.

(S7) H. B. Zhang, P. F. An, W. Zhou, B. Y. Guan, P. Zhang, J. C. Dong and X. W. Lou, *Sci. Adv.*, 2018, **4**, 9.

(S8) Y. Wang, L. Chen, X. Yu, Y. Wang and G. Zheng, *Adv. Energy Mater*., 2017, **7**, 1601390.

(S9) J. Fan, K. Qi, L. Zhang, H. Zhang, S. Yu and X. Cui, *ACS Appl. Mater. Interfaces*, 2017, **9**, 18008-18014.

(S10) K. Tang, X. F. Wang, Q. Li and C. L. Yan, *Adv. Mater.*, 2018, **30**, 170477.

(S11) J.-Q. Chi, J.-Y. Xie, W.-W. Zhang, B. Dong, J.-F. Qin, X.-Y. Zhang, J.-H. Lin, Y.-M. Chai and C.-G. Liu, *ACS Appl. Mater. Interfaces*, 2019, **11**, 4047-4056.

(S12) V.-T. Nguyen, N.-A. Nguyen, Y. Ali, Q. C. Tran and H.-S. Choi, *Carbon*, 2019, **146**, 116-124.

(S13) L. Xie, X. Ren, Q. Liu, G. Cui, R. Ge, A. M. Asiri, X. Sun, Q. Zhang and L. Chen, *J. Mater. Chem. A*, 2018, **6**, 1967-1970.

(S14) J. Zhang, P. Liu, G. Wang, P. P. Zhang, X. D. Zhuang, M. W. Chen, I. M. Weidinger and X. L. Feng, *J. Mater. Chem. A*, 2017, **5**, 25314-25318.

(S15) W. Chen, J. Pei, C.-T. He, J. Wan, H. Ren, Y. Zhu, Y. Wang, J. Dong, S. Tian, W.-C. Cheong, S. Lu, L. Zheng, X. Zheng, W. Yan, Z. Zhuang, C. Chen, Q. Peng, D. Wang and Y. Li, *Angew. Chem. Int. Ed.*, 2017, **129**, 16302-16306.

(S16) R. Luo, M. Luo, Z. Wang, P. Liu, S. Song, X. Wang and M. Chen, *Nanoscale*, 2019, **11**, 7123-7128.

(S17) L. Cao, Q. Luo, W. Liu, Y. Lin, X. Liu, Y. Cao, W. Zhang, Y. Wu, J. Yang, T. Yao and S. Wei, *Nat. Catal.*, 2019, **2**, 134-141.

(S18) Y. Qu, B. Chen, Z. Li, X. Duan, L. Wang, Y. Lin, T. Yuan, F. Zhou, Y. Hu, Z. Yang, C. Zhao, J. Wang, C. Zhao, Y. Hu, G. Wu, Q. Zhang, Q. Xu, B. Liu, P. Gao, R. You, W. Huang, L. Zheng, L. Gu, Y. Wu and Y. Li, *J. Am. Chem. Soc*., 2019, **141**, 4505-4509.

(S19) J. Yang, B. Chen, X. Liu, W. Liu, Z. Li, J. Dong, W. Chen, W. Yan, T. Yao, X. Duan, Y. Wu and Y. Li, *Angew. Chem., Int. Ed*., 2018, **57**, 9495-9500.

(S20) D. Liu, X. Li, S. Chen, H. Yan, C. Wang, C. Wu, Y. A. Haleem, S. Duan, J. Lu, B. Ge, P. M. Ajayan, Y. Luo, J. Jiang and L. Song, *Nat. Energy*, 2019, **4**, 512-518.

(S21) L. Ji, P. Yan, C. Zhu, C. Ma, W. Wu, C. Wei, Y. Shen, S. Chu, J. Wang, Y. Du, J. Chen, X. Yang and Q. Xu, *Appl. Catal. B*, 2019, **251**, 87-93.

(S22) M. D. Hossain, Z. Liu, M. Zhuang, X. Yan, G.-L. Xu, C. A. Gadre, A. Tyagi, I. H. Abidi, C.-J. Sun, H. Wong, A. Guda, Y. Hao, X. Pan, K. Amine and Z. Luo, *Adv. Energy Mater.*, 2019, **9**, 1803689.